

Data Mapping and Finite Difference Learning

Jiangsheng You

jshyou@gmail.com

Abstract

Restricted Boltzmann machine (RBM) is a two-layer neural network constructed as a probabilistic model and its training is to maximize a product of probabilities by the contrastive divergence (CD) scheme. In this paper a data mapping is proposed to describe the relationship between the visible and hidden layers and the training is to minimize a squared error on the visible layer by a finite difference learning. This paper presents three new properties in using the RBM: 1) nodes on the visible and hidden layers can take real-valued matrix data without a probabilistic interpretation; 2) the famous CD1 is a finite difference approximation of the gradient descent; 3) the activation can take non-sigmoid functions such as identity, relu and softsign. The data mapping provides a unified framework on the dimensionality reduction, the feature extraction and the data representation pioneered and developed by Hinton and his colleagues. As an approximation of the gradient descent, the finite difference learning is applicable to both directed and undirected graphs. Numerical experiments are performed to verify these new properties on the very low dimensionality reduction, the collinearity of timer series data and the use of flexible activations.

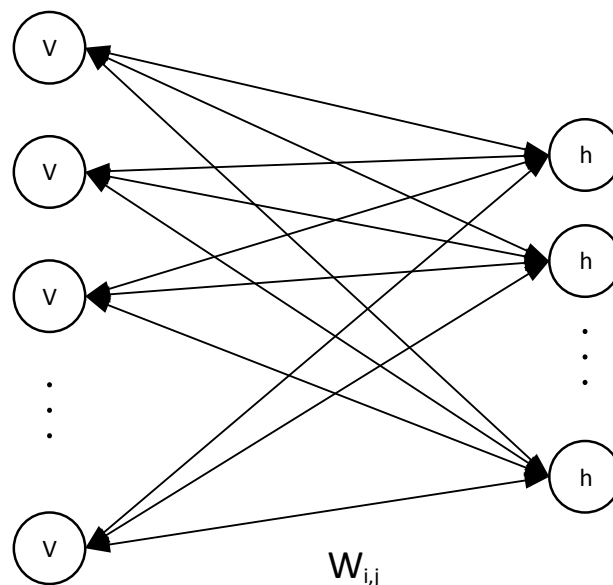
Keywords: Restricted Boltzmann machine, data mapping, squared error, contrastive divergence, gradient descent and finite difference learning.

I. Data mapping and energy function

Some new properties of RBM are presented in this paper based on recent study on the deep learning from [1] and many internet blogs on the algorithms and philosophies of the artificial intelligence. The RBM was first introduced under the name of Harmonium by Smolensky P. in [2]. Hinton G. E. and his colleagues investigated the contrastive divergence (CD) learning method to make the RBM more efficient for dimensionality reduction and feature extraction [3, 4]. Traditionally the RBM has been studied using the probabilistic model [5]. During the comprehension of the probabilistic explanation of RBM, the author recalled a similar iteration scheme to implement the expectation maximization (EM) algorithm for maximum likelihood in the domain of image reconstruction from projections [6]. Back then the authors could not provide a mathematical explanation for the iteration scheme though the computations were efficient and the results were comparable to the standard implementation. During reading the blog [7], the author started thinking of establishing an energy function on the visible layer following the ideas from the algebraic reconstruction technique (ART) of [8] and the backprojection implementation of the EM algorithm [9, 10]. This is how this paper was originated.

Before discussing more details on the RBM, we give a quick recollection of the neural network architecture. From the early multiple layer perception (MLP) to the recent breakthrough on the deep networks such as convolutional neural network (CNN) and recurrent neural network (RNN), the neural response is traditionally defined as a feedforward process though RNN adopts the concept of self-response within the same unit. In the real world, the responses of neurons are always mutually interactive and different neurons may have different activation responses. The RBM is one of networks that are defined as a bipartite graph to reflect the mutual responses as shown below.

Symmetrical bipartite graph with shared weights



The nodes on the left side construct the visible layer that represents the input and the nodes on the right side construct the hidden layer that represents features or latent variables. The weights are shared by the feedforward propagation and the backward reconstruction. The RBM is developed as a probabilistic model on the visible and hidden layers, for example, Bernoulli or Gaussian distributions are commonly used to describe the data. The existing teaching of RBM uses the stochastic theory that is based on Markov random

field, and Hinton suggested that the hidden layer is better using binary distribution. Especially the RBM may not be stable if the Gaussian distribution is used for both visible and hidden layers.

In the image reconstruction from projections, the relationship between image and projection is associated by a coefficient matrix which is used in the projection from image and the backprojection to the image [8, 9]. Instead of establishing a maximum likelihood on the hidden layer, the author studied the idea of treating the hidden layer as latent variables and directly establishing an energy function on the visible layer. Following this idea, the RBM is interpreted as a pair of data mapping between the visible and hidden layers without a probabilistic model to describe the data.

Let $R^m, R^n, R^{m \times n}$ denote Euclidean spaces with dimensions of m, n , and $m \times n$ correspondingly. Vectors $\vec{X} \in R^m$ and $\vec{Y} \in R^n$ stand for the data on visible and hidden layers, respectively. Matrix $\mathbf{W} \in R^{n \times m}$ represents a linear transform from R^m to R^n . Let $\vec{A}_v(\cdot), \vec{A}'_v(\cdot), \vec{A}_h(\cdot)$ and $\vec{A}'_h(\cdot)$ denote activation functions and their derivatives for visible and hidden layers, depending on the context. In this paper activation functions are defined from R^m to R^m or R^n to R^n as a scalar function on each node, for example, $\vec{A}_v(\cdot)$ is understood as $\{\vec{A}_{v,1}(x_1), \dots, \vec{A}_{v,m}(x_m)\}^T$, here superscript T stands for the transpose operation and $\vec{A}_{v,k}(x_k), k = 1, \dots, m$, may be different on different nodes. The mathematical notations follow the convention outlined in [1]. As a data mapping from the visible layer to the hidden layer, the output \vec{Y} and the input \vec{X} with bias \vec{B}_h can be described as

$$\vec{Y} = \vec{A}_h(\mathbf{W}\vec{X} + \vec{B}_h) \quad (1)$$

Unlike the interpretation of \vec{Y} by the Bernoulli distribution in [1, 3, 4], we simply treat the above relation as a mathematical function from R^m to R^n without attaching a probability to $\vec{A}_h(\cdot)$. This leads to the freedom that the range of \vec{Y} can be real-valued and the activation $\vec{A}_h(\cdot)$ may take any form that is proper to solve the problem under consideration. Vector \vec{Y} may be understood as the dimension-reduced version of \vec{X} , the features extracted from \vec{X} or other representations of \vec{X} . Define the reconstruction from the hidden layer with bias \vec{B}_v as

$$\vec{X} = \vec{A}_v(\mathbf{W}^T\vec{Y} + \vec{B}_v) \quad (2)$$

The pair of \vec{X} and \vec{Y} construct a data mapping between the visible and hidden layers through the shared weights \mathbf{W} . Both \vec{X} and \vec{Y} can be real-valued vector and activations $\vec{A}_v(\cdot)$ and $\vec{A}_h(\cdot)$ may admit negative or complex values without a probabilistic representation. In mathematics, (2) can be regarded as the counter response of the visible layer through a transpose of \mathbf{W} . If we wish the counter response to be close to the original input, we consider the energy function as follows

$$E(\mathbf{W}, \vec{B}_h, \vec{B}_v) = \frac{1}{2} \|\vec{A}_v(\mathbf{W}^T\vec{A}_h(\mathbf{W}\vec{X} + \vec{B}_h) + \vec{B}_v) - \vec{X}\|^2 \quad (3)$$

and solve the minimization problem:

$$\operatorname{argmin}_{\mathbf{W}, \vec{B}_h, \vec{B}_v} E(\mathbf{W}, \vec{B}_h, \vec{B}_v) \quad (4)$$

Please keep in mind that the squared error (3) does not require any probabilistic assumption on the hidden layer except being used as an intermittent layer. We may compare the reconstructed and original data after the activation like the recirculation of network in [11] by

$$E(\mathbf{W}, \vec{B}_h, \vec{B}_v) = \frac{1}{2} \|\vec{A}_v(\mathbf{W}^T\vec{A}_h(\mathbf{W}\vec{X} + \vec{B}_h) + \vec{B}_v) - \vec{A}_v(\vec{X})\|^2 \quad (5)$$

Mathematically (5) may be more plausible because the squared error is defined in the same range of activation \overrightarrow{A}_v , but it has not become popular in the research community.

As described in [1, 5], the bipartite graph is primarily studied in the literature by using the probabilistic model. The classic teaching of binary RBM is considering the marginal probability

$$P(\mathbf{v}; \mathbf{a}, \mathbf{b}, \mathbf{W}) = \frac{1}{Z} \sum_{\mathbf{h}} \exp(\mathbf{a}^T \mathbf{v} + \mathbf{b}^T \mathbf{h} + \mathbf{h}^T \mathbf{W} \mathbf{v}) \quad (6)$$

where Z is the partition function derived from all possible configurations, \mathbf{a} , \mathbf{b} , and \mathbf{W} are parameters. The training is to find the solution of the maximized product of probabilities

$$\operatorname{argmax}_{\mathbf{W}, \mathbf{a}, \mathbf{b}} \prod_{\mathbf{v}} P(\mathbf{v}; \mathbf{a}, \mathbf{b}, \mathbf{W}) \quad (7)$$

Equation (7) is in the form of exponential functions and is intractable. Hinton first studied the contrastive divergence (CD) learning procedure and more investigations and the history are referenced to [1, 5]. The famous CD1 was shown in [4] to be efficient for dimensionality reduction and triggered the revival of deep learning and the more breakthroughs since then.

In this paper a finite difference learning procedure is proposed as the approximation of the gradient descent to solve the minimization of (3) and (5). Under certain condition, the finite difference learning is the same as CD1 but the derivation in this paper does not use the probabilistic model. Without needing a probabilistic interpretation, both the visible and hidden layers can take real-valued data in the same way. By extending (1) and (2) to block matrix operation, \vec{X} and \vec{Y} can be matrix on both visible and hidden layers as well. Moreover, the finite difference learning can be used for the directed graph like MLP to avoid calculating the derivatives required in the gradient descent. Numerical results are presented to solve (4) for linear and nonlinear data representations. It is worth mentioning that data mapping leads to a new type of linear methods for dimensionality reduction and independent component analysis (ICA) without using the covariance.

II. Difference learning and gradient descent

In this section we first derive the gradient descent method to estimate \mathbf{W} , $\overrightarrow{B}_h, \overrightarrow{B}_v$ for (4), and then investigate the relationship between a finite difference learning and the gradient descent method. Let \odot denote the element-wise multiplication between two vectors and introduce three definitions

$$\vec{Y} = \mathbf{W} \vec{X} + \overrightarrow{B}_h, \quad \vec{X} = \mathbf{W}^T \vec{Y} + \overrightarrow{B}_v \quad \text{and} \quad \overrightarrow{\Delta X} = \overrightarrow{A}_v(\vec{X}) - \vec{X} \quad (8)$$

By linear algebra and multivariable calculus, we obtain the gradients of (3) as follows:

$$\frac{\partial}{\partial \overrightarrow{B}_v} E(\mathbf{W}, \overrightarrow{B}_h, \overrightarrow{B}_v) = \overrightarrow{A}'_v(\vec{X}) \odot \overrightarrow{\Delta X} \quad (9)$$

$$\frac{\partial}{\partial \overrightarrow{B}_h} E(\mathbf{W}, \overrightarrow{B}_h, \overrightarrow{B}_v) = \overrightarrow{A}'_h(\vec{Y}) \odot [\mathbf{W}(\overrightarrow{A}'_v(\vec{X}) \odot \overrightarrow{\Delta X})] \quad (10)$$

$$\frac{\partial}{\partial \mathbf{W}} E(\mathbf{W}, \overrightarrow{B}_h, \overrightarrow{B}_v) = \vec{Y} [\overrightarrow{A}'_v(\vec{X}) \odot \overrightarrow{\Delta X}]^T + \{\overrightarrow{A}'_h(\vec{Y}) \odot [\mathbf{W}(\overrightarrow{A}'_v(\vec{X}) \odot \overrightarrow{\Delta X})]\} \vec{X}^T \quad (11)$$

The derivation of equations (9-11) is straightforward by using the derivative of vector inner product and the product rule in calculus to find the derivatives of products of two or more functions. Let \overrightarrow{X}_0 stand for the original input data on the visible layer, for an initial estimate $[\mathbf{W}_0, \overrightarrow{B}_{h,0}, \overrightarrow{B}_{v,0}]$ and a scalar learning rate γ , we obtain the gradient descent (GD) learning steps for (4) as follows:

$$1. \quad \vec{Y}_0 = \mathbf{W}_0 \overrightarrow{X}_0 + \overrightarrow{B}_{h,0} \quad \text{and} \quad \vec{Y}_0 = \overrightarrow{A}_h(\vec{Y}_0) \quad (\text{GD-1})$$

$$2. \quad \overrightarrow{X}_1 = \mathbf{W}_0^T \overrightarrow{Y}_0 + \overrightarrow{B}_{v,0} \text{ and } \overrightarrow{X}_1 = \overrightarrow{A}_v(\overrightarrow{X}_1) \quad (\text{GD-2})$$

$$3. \quad \text{Let } \overrightarrow{\delta X} = \overrightarrow{A}'_v(\overrightarrow{X}_1) \odot (\overrightarrow{X}_1 - \overrightarrow{X}_0), \text{ then update } [\mathbf{W}_0, \overrightarrow{B}_{h,0}, \overrightarrow{B}_{v,0}] \text{ to } [\mathbf{W}_1, \overrightarrow{B}_{h,1}, \overrightarrow{B}_{v,1}] \text{ by} \quad (\text{GD-3})$$

$$\text{a. } \overrightarrow{B}_{v,1} = \overrightarrow{B}_{v,0} - \gamma \overrightarrow{\delta X} \quad (\text{GD-3a})$$

$$\text{b. } \overrightarrow{B}_{h,1} = \overrightarrow{B}_{h,0} - \gamma \overrightarrow{A}'_h(\overrightarrow{Y}_0) \odot [\mathbf{W}_0 \overrightarrow{\delta X}] \quad (\text{GD-3b})$$

$$\text{c. } \mathbf{W}_1 = \mathbf{W}_0 - \gamma \{ \overrightarrow{Y}_0 \overrightarrow{\delta X}^T + [\overrightarrow{A}'_h(\overrightarrow{Y}_0) \odot (\mathbf{W}_0 \overrightarrow{\delta X})] \overrightarrow{X}_0^T \} \quad (\text{GD-3c})$$

$$4. \quad \text{Replace } [\mathbf{W}_0, \overrightarrow{B}_{h,0}, \overrightarrow{B}_{v,0}] \text{ by } [\mathbf{W}_1, \overrightarrow{B}_{h,1}, \overrightarrow{B}_{v,1}] \text{ and go to step 1} \quad (\text{GD-4})$$

Notice that the above learning procedure follows the classical gradient descent in solving an optimization problem. It is straightforward to obtain that the gradient descent for minimizing (5) is virtually identical to the steps from (GD-1) to (GD-4) through replacing $\overrightarrow{X}_1 - \overrightarrow{X}_0$ by $\overrightarrow{X}_1 - \overrightarrow{A}_v(\overrightarrow{X}_0)$.

For the simplicity, we assume that $\overrightarrow{A}_v(\cdot)$ is the identity and $(\overrightarrow{X}_1 - \overrightarrow{X}_0)$ is small enough so that the second-order error can be ignored. Let $\overrightarrow{Y}_1 = \overrightarrow{A}_h(\mathbf{W}_0 \overrightarrow{X}_0 + \overrightarrow{B}_{h,0})$, we obtain

$$\overrightarrow{Y}_1 - \overrightarrow{Y}_0 \approx \overrightarrow{A}'_h(\overrightarrow{Y}_0) \odot [\mathbf{W}_0 (\overrightarrow{X}_1 - \overrightarrow{X}_0)] \quad (12)$$

$$\overrightarrow{Y}_1 \overrightarrow{X}_1^T - \overrightarrow{Y}_0 \overrightarrow{X}_0^T \approx \overrightarrow{Y}_0 (\overrightarrow{X}_1 - \overrightarrow{X}_0)^T + \{ \overrightarrow{A}'_h(\overrightarrow{Y}_0) \odot [\mathbf{W}_0 (\overrightarrow{X}_1 - \overrightarrow{X}_0)] \} \overrightarrow{X}_0^T \quad (13)$$

Here $\{ \overrightarrow{A}'_h(\overrightarrow{Y}_0) \odot [\mathbf{W}_0 (\overrightarrow{X}_1 - \overrightarrow{X}_0)] \} \overrightarrow{X}_1^T \approx \{ \overrightarrow{A}'_h(\overrightarrow{Y}_0) \odot [\mathbf{W}_0 (\overrightarrow{X}_1 - \overrightarrow{X}_0)] \} \overrightarrow{X}_0^T$ is used in the derivation of (13). Notice that the left sides of (12) and (13) are the CD1 scheme while the right sides are the classical GD steps. Thus we conclude that CD1 is a finite difference approximation of the gradient descent for (3). It is a miracle and the beauty of mathematics that CD1 increases the productized probability (7) and decreases the energy function (3) as a harmonium.

Now we extend the CD1 to a finite difference learning procedure. For a given initial estimate of $[\mathbf{W}_0, \overrightarrow{B}_{h,0}, \overrightarrow{B}_{v,0}]$, we have the initial data mapping pair $[\overrightarrow{X}_0, \overrightarrow{Y}_0]$. After performing another round of data mapping, we obtain a new pair $[\overrightarrow{X}_1, \overrightarrow{Y}_1]$. The idea of the finite difference learning is to update the initial estimate $[\mathbf{W}_0, \overrightarrow{B}_{h,0}, \overrightarrow{B}_{v,0}]$ by compensating the difference from two rounds of data mapping with the following scheme

$$\overrightarrow{B}_{v,1} = \overrightarrow{B}_{v,0} - \overrightarrow{\gamma}_v \odot (\overrightarrow{X}_1 - \overrightarrow{X}_0) \quad (\text{FD-1})$$

$$\overrightarrow{B}_{h,1} = \overrightarrow{B}_{h,0} - \overrightarrow{\gamma}_h \odot (\overrightarrow{Y}_1 - \overrightarrow{Y}_0) \quad (\text{FD-2})$$

$$\mathbf{W}_1 = \mathbf{W}_0 - \overrightarrow{\gamma}_W \odot (\overrightarrow{Y}_1 \overrightarrow{X}_1^T - \overrightarrow{Y}_0 \overrightarrow{X}_0^T) \quad (\text{FD-3})$$

Here $\overrightarrow{\gamma}_*$ is the element-dependent learning rate. Notice that the expression of the above finite difference (FD) learning was originally derived in [3] as the famous CD1 scheme. Here we point out that (FD) is an approximation of the GD around the local minimum from (12) and (13) and does degenerate to the classical GD when activations are the identity in the case of linear transforms. From many numerical experiments in our tests with MINIST dataset, no noticeable difference has been identified between using GD and FD except that the learning rate may need to be smaller in using (FD) to avoid numerical overflow. The RBM as a data mapping has these properties:

- 1) Both \overrightarrow{X} and \overrightarrow{Y} are real-valued data and can be configured as matrix as shown in next section.
- 2) When the activations are the identity, the RBM becomes a new model to perform linear factor analysis without using the covariance criterion.
- 3) The FD is an approximation of the gradient descent.

Next we extend (FD) to the feedforward network. Assume that \mathbf{W} stands for the weights and \vec{Y} is the target, we consider the following energy function

$$E(\mathbf{W}, \vec{B}) = \frac{1}{2} \|\vec{A}(\mathbf{W}\vec{X} + \vec{B}) - \vec{Y}\|^2 \quad (14)$$

where \vec{B} is the bias and \vec{A} stands for the activation. In the context of image reconstruction from projections, \vec{A} is the identity, \vec{B} is zero and \mathbf{W} are the projection coefficients, the goal is to reconstruct \vec{X} for given \vec{Y} . In MLP, \vec{B} is the bias and \mathbf{W} are the network weights to be estimated. If the layer is in the middle of deep networks, \vec{X} needs to be estimated to decrease the error on the previous layer. In all these cases, let \vec{Y}_0 stand for the target vector, for an initial estimate of $\{\vec{X}_0, \vec{B}_0, \mathbf{W}_0\}$ and $\vec{Y}_1 = \vec{A}(\mathbf{W}_0\vec{X}_0 + \vec{B}_0)$, we express the gradient descent method as follows:

$$\vec{X}_1 = \vec{X}_0 - \gamma \vec{A}'(\vec{Y}_1) \odot [\mathbf{W}_0^T (\vec{Y}_1 - \vec{Y}_0)] \quad (\text{GD-a})$$

$$\vec{B}_1 = \vec{B}_0 - \gamma \vec{A}'(\vec{Y}_1) \odot (\vec{Y}_1 - \vec{Y}_0) \quad (\text{GD-b})$$

$$\mathbf{W}_1 = \mathbf{W}_0 - \gamma [\vec{A}'(\vec{Y}_1) \odot (\vec{Y}_1 - \vec{Y}_0)] \vec{X}_0^T \quad (\text{GD-c})$$

The corresponding FD learning for (14) can be expressed in the following steps:

$$\vec{X}_1 = \vec{X}_0 - \vec{\gamma} \odot [\mathbf{W}_0^T (\vec{Y}_1 - \vec{Y}_0)] \quad (\text{FD-a})$$

$$\vec{B}_1 = \vec{B}_0 - \vec{\gamma} \odot (\vec{Y}_1 - \vec{Y}_0) \quad (\text{FD-b})$$

$$\mathbf{W}_1 = \mathbf{W}_0 - [\vec{\gamma} \odot (\vec{Y}_1 - \vec{Y}_0)] \vec{X}_0^T \quad (\text{FD-c})$$

Notice that FD becomes GD when activation \vec{A} is the identity for the linear least square.

Remark. The variable learning rate in FD scheme may be useful to speed up the convergence around the local minimum through adjusting the rate along different directions. The gradient is not needed so non-smooth activations like relu can be used in the network architecture. If more rounds of data mapping are performed, a CDn-like procedure can be constructed following the scheme described in [3-5]. In mathematics, the gradient is the local property of a function while the difference between data mappings can reflect the changes from a small or large area. Human vision is more sensitive to the difference regardless of the size of area, the difference learning may be more reflective of the human vision perception than the pure mathematical procedure to find a minimum.

III. Numerical experiments of linear representation

In this section we assume activations $\vec{A}_h(\cdot)$ and $\vec{A}_v(\cdot)$ are the identity, the data mapping defined by (1) and (2) is a linear factor model with the following energy function

$$E(\mathbf{W}, \vec{B}_h, \vec{B}_v) = \frac{1}{2} \|\mathbf{W}^T \mathbf{W} \vec{X} + \mathbf{W}^T \vec{B}_h + \vec{B}_v - \vec{X}\|^2 \quad (15)$$

Principal component analysis (PCA) has been one of the most important linear methods for dimensionality reduction through minimizing the covariance. Here we minimize the L^2 norm between the original data and reconstructed data among all the linear mappings. To our knowledge, energy function (15) has not been explored in the literature for dimensionality reduction and independent component analysis. For the linear transform, the FD and GD schemes are the same (15) as follows

$$\vec{B}_{v,1} = \vec{B}_{v,0} - \gamma (\vec{X}_1 - \vec{X}_0) \quad (\text{FDL-1})$$

$$\vec{B}_{h,1} = \vec{B}_{h,0} - \gamma \mathbf{W}_0 (\vec{X}_1 - \vec{X}_0) \quad (\text{FDL-2})$$

$$\mathbf{W}_1 = \mathbf{W}_0 - \gamma \{ \vec{Y}_0 (\vec{X}_1 - \vec{X}_0)^T + \mathbf{W}_0 (\vec{X}_1 - \vec{X}_0) \vec{X}_0^T \} \quad (\text{FDL-3})$$

It has been shown in [4] and many subsequent works that the stacked RBMs as an autoencoder can outperform PCA on dimensionality reduction. In this section we present three examples of using (15) for dimensionality reduction, independent component analysis and feature extraction. The purpose of numerical experiments is to show how to configure the network architecture instead of quantitative analysis and comparison study over other existing methods.

A. Single RBM for linear dimensionality reduction

In this subsection MNIST images are used to verify the difference learning scheme from (FDL-1) to (FDL-3). From 10000 test images of MNIST, we use 9000 images for learning and the remaining 1000 images for testing. The input dimension is $784=28 \times 28$ and the output dimension is $49=7 \times 7$ which is small for a single layer. Two sets of results are shown below, one is for all 10 digits and the other includes 10 visually different images of digit 2. With compression ratio of 16, the reconstructed images are visually close to the original images. More detailed quantitative analysis may be needed to measure the reconstruction accuracy and to characterize the feature patterns.

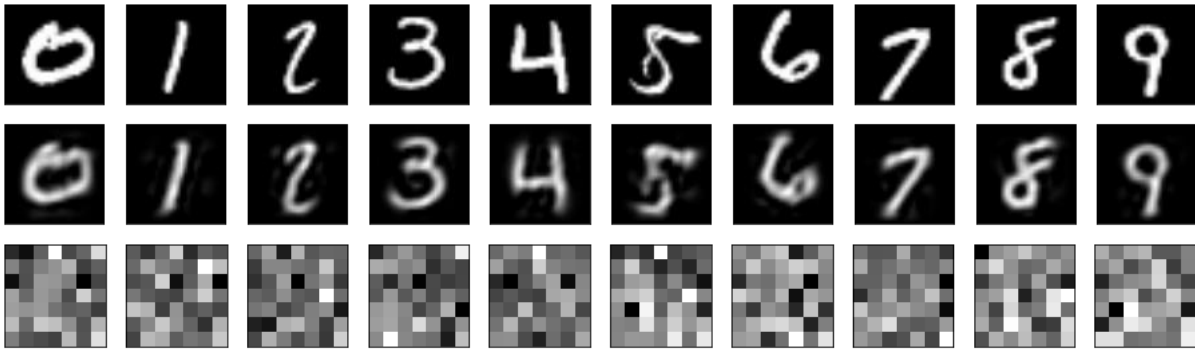


Fig 1. row 1: original images, row 2: reconstructed images and row 3: projected features

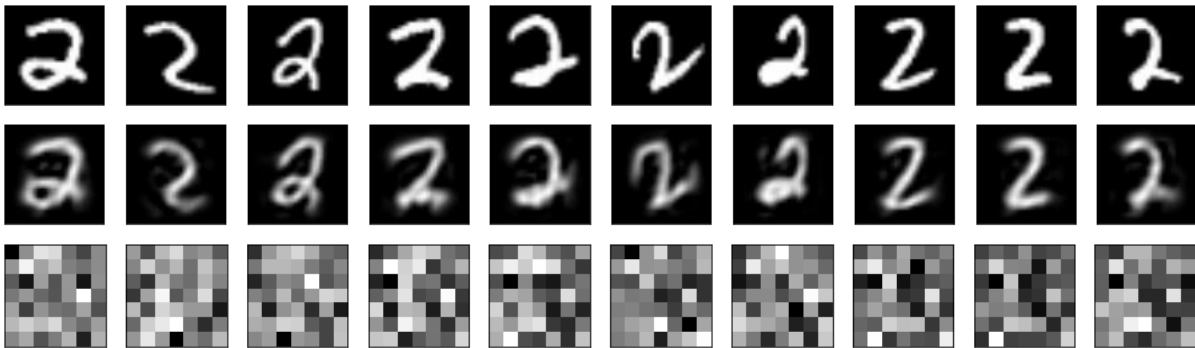


Fig 2. row 1: original images, row 2: reconstructed images and row 3: projected features

Analyzing the feature patterns is a very interesting topic and may be potentially important to improve the digit classification. The quantitative comparison against PCA may be another important topic to investigate if any advantage of data mapping can offer.

B. Single RBM for collinearity analysis

In this subsection we configure (15) to find the independent components among random vectors as studied in [12]. Using the block matrix operations, the data mappings (1) and (2) can be described as:

1. Let each element of \vec{X} and \vec{Y} be a vector with the same dimension.

2. The projection formula (1) is defined as

$$\bar{Y}^i = \sum_j w_{i,j} \bar{X}^j + \bar{B}_h^i \quad (16-1)$$

here \bar{X}^j and \bar{B}_h^j are the j -th element of input and bias, respectively. \bar{Y}^i is the i -th element of output. Notice that the weights continue to be a matrix.

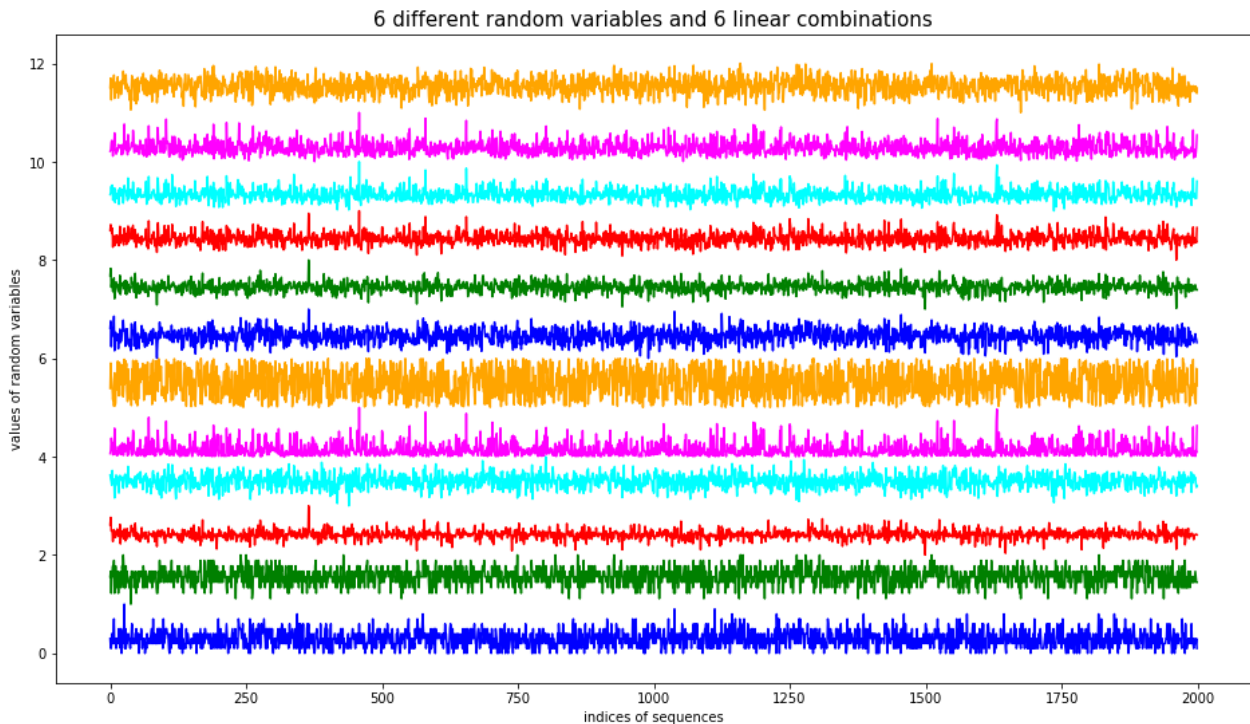
3. Let \bar{B}_v^j be the bias, the reconstruction formula (2) is defined as

$$\bar{X}^j = \sum_i w_{i,j} \bar{Y}^i + \bar{B}_v^j \quad (16-2)$$

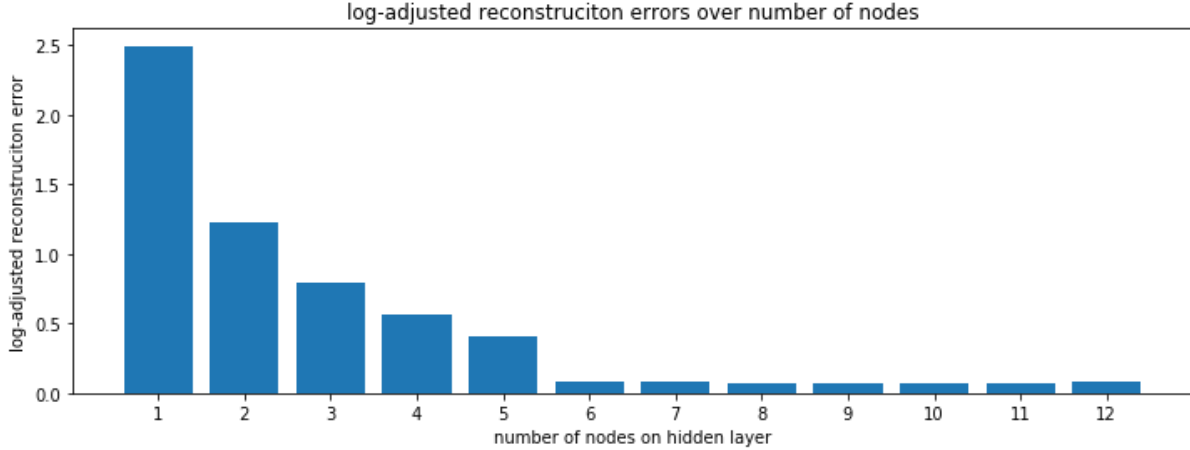
The matrix operations in (FDL-2) and (FDL-3) shall follow the block matrix operations defined by (16-1) and (16-2), respectively. We first generate 6 different random series by Poisson, binomial, Laplace, Gaussian, exponential and uniform distributions, and then make 6 random series by combining these 6 independent random series. The details in Python code are defined as follows:

```
seq_len      = 2000
seq_data[0]  = np.random.poisson(3.0, seq_len)
seq_data[1]  = np.random.binomial(10.0, 0.6, seq_len)
seq_data[2]  = np.random.laplace(-1.0, 1.0, seq_len)
seq_data[3]  = np.random.normal(0.5, 1.0, seq_len)
seq_data[4]  = np.random.exponential(2.0, seq_len)
seq_data[5]  = np.random.uniform(-2.0, 2.0, seq_len)
seq_data[6]  = seq_data[0]*0.25+seq_data[1]*0.75+seq_data[2]*0.50
seq_data[7]  = seq_data[1]*0.30+seq_data[2]*0.70+seq_data[3]*0.50
seq_data[8]  = seq_data[2]*0.45+seq_data[3]*0.55+seq_data[4]*0.35
seq_data[9]  = seq_data[3]*0.60+seq_data[4]*0.40+seq_data[5]*0.20
seq_data[10] = seq_data[4]*0.50+seq_data[5]*0.35+seq_data[0]*0.45
seq_data[11] = seq_data[5]*0.40+seq_data[0]*0.10+seq_data[1]*0.60
```

The plot of these 12 sequences is shown below:



The length of each sequence is 2000 and we use the subsequence of length 50 and the stride length of 20 to generate the training samples. In this configuration, \vec{X} has 12 nodes with each being a 50-dimensional vector, \vec{Y} has variable numbers of nodes with each being a 50-dimensional vector. There are 6 independent series, if the number of nodes for \vec{Y} is strictly less than 6, then the reconstruction won't be accurate but an accurate reconstruction exists when the number of nodes for \vec{Y} is 6 or larger. Here is the chart of reconstruction errors over the number of nodes with 100 epochs.



Hereafter the log-adjusted error is $-1.0/\log(mse)$, mse stands for the mean squared error. The author remarks that the configuration of (16-1) and (16-2) can be used to find the number of independent components and the coefficients between the independent and non-independent components if the correlation is linear.

C. Single RBM for feature extraction of random sequences

More detailed analysis of the feature extraction by RBM for images can be found in [13]. For MNIST dataset, Hinton and his colleagues performed many interesting results of the binary grid features. In this subsection we configure the RBM architecture for feature extraction of random sequences. Using the block matrix operations, the data mappings (1) and (2) can be described as:

1. Let each element of \vec{X} and \vec{Y} be a vector with different dimensions.
2. The projection formula (1) is defined as

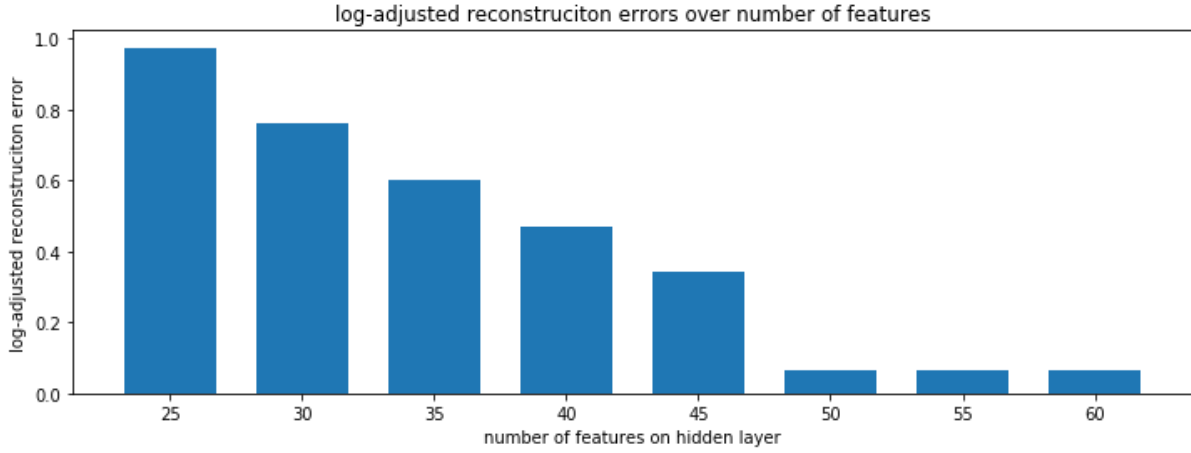
$$\vec{Y}^i = \mathbf{W}\vec{X}^i + \vec{B}_h^i \quad (17-1)$$

here \vec{X}^i and \vec{B}_h^i are the i -th element of input and bias as a vector, respectively. \vec{Y}^i is the i -th element of output. Notice that the weights continue to be a matrix.

3. The reconstruction formula (2) is defined as

$$\vec{X}^i = \mathbf{W}^T\vec{Y}^i + \vec{B}_v^i \quad (17-2)$$

Similarly, the matrix operations in (FDL-2) and (FDL-3) shall follow the block matrix operation defined by (17-1) and (17-2), respectively. We continue to use the samples generated in the previous subsection but both the visible and hidden layers have 12 nodes with different dimensions. For feature vector dimensions of 25, 30, 35, 40, 45, 50, 55 and 60, the reconstruction errors are shown in the following chart:



For random data there is virtually not much compression to achieve, so the reconstruction errors are significant if the number of features is smaller than the original length but the reconstruction error becomes neglect when the number of features is equal or larger than the sequence length.

IV. Numerical experiments of nonlinear representation

Throughout this section we assume that $\overrightarrow{A}_v(\cdot)$ is either the identity or relu, and $\overrightarrow{A}_h(\cdot)$ is softsign which has the value range in $[-1, 1]$ and a quadratic decay. If $\overrightarrow{A}_v(\cdot)$ is the identity, the energy function (3) becomes

$$E(\mathbf{W}, \overrightarrow{B}_h, \overrightarrow{B}_v) = \frac{1}{2} \|\mathbf{W}^T \overrightarrow{A}_h(\mathbf{W}\vec{X} + \overrightarrow{B}_h) + \overrightarrow{B}_v - \vec{X}\|^2 \quad (18)$$

The FD scheme for (18) is expressed in (FD-1) to (FD-3) and the GD scheme of (GD-3a) to (GD-3c) can be simplified as

$$\overrightarrow{B}_{v,1} = \overrightarrow{B}_{v,0} - \gamma(\overrightarrow{X}_1 - \overrightarrow{X}_0) \quad (\text{GDN-1})$$

$$\overrightarrow{B}_{h,1} = \overrightarrow{B}_{h,0} - \gamma \overrightarrow{A}'_h(\overrightarrow{Y}_0) \odot [\mathbf{W}_0(\overrightarrow{X}_1 - \overrightarrow{X}_0)] \quad (\text{GDN-2})$$

$$\mathbf{W}_1 = \mathbf{W}_0 - \gamma \{ \overrightarrow{Y}_1(\overrightarrow{X}_1 - \overrightarrow{X}_0)^T + [\overrightarrow{A}'_h(\overrightarrow{Y}_0) \odot (\mathbf{W}_0(\overrightarrow{X}_1 - \overrightarrow{X}_0))] \overrightarrow{X}_0^T \} \quad (\text{GDN-3})$$

For theoretical curiosity and practical applications with real-valued input data, we present two examples of using the softsign activation to show that both RBM and stacked RBMs do produce desired results for floating numbers on both visible and hidden layers.

A. Single RBM with nonlinear softsign activation

In this subsection we present some reconstruction results for nonlinear mapping with softsign activation. More specifically, the activation on the hidden layer is softsign and the activation is relu on the visible layer. Hereafter we use RBM(m, n) to represent one single RBM with input dimension of m and hidden layer dimension of n , for example RBM(784, 49) is the configuration for MNIST with target dimension of 49. The results are shown below.

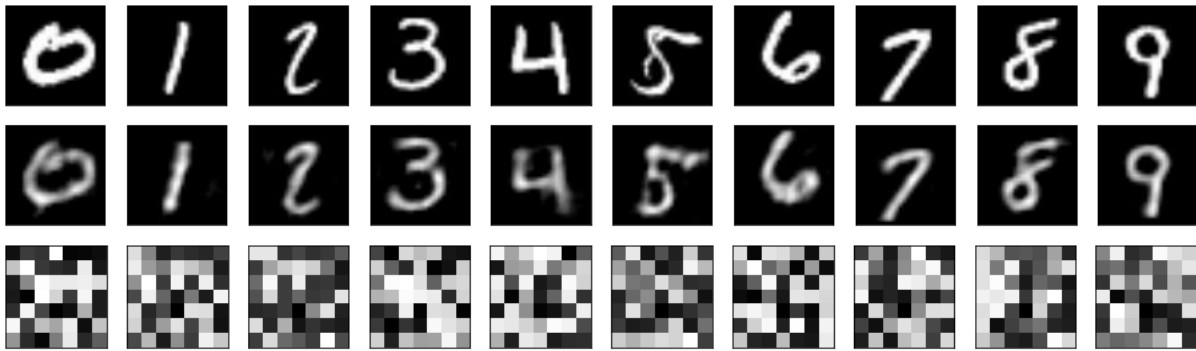


Fig 3. row 1: original images, row 2: reconstructed images and row 3: projected features

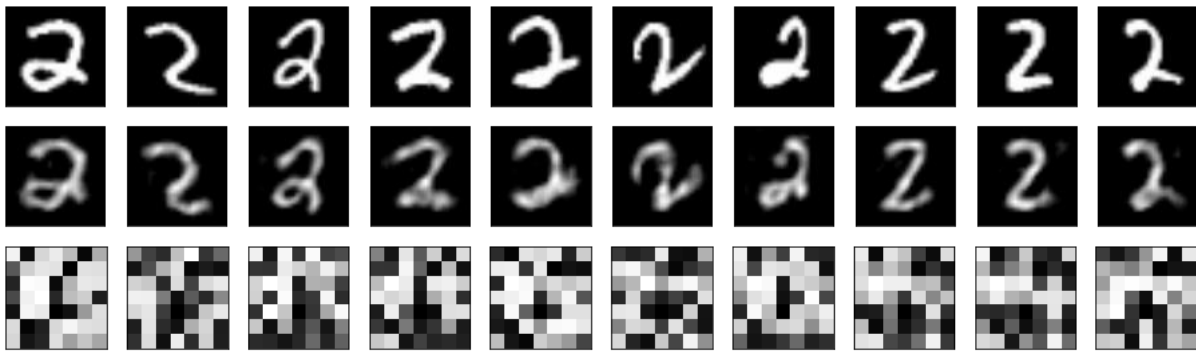


Fig 4. row 1: original images, row 2: reconstructed images and row 3: projected features

The purpose of the numerical results is to show the flexible choice of the activation on both visible and hidden layers. It is an important topic to analyze the accuracy metrics among different activations and compare the difference between linear mapping and nonlinear mapping.

B. Stacked RBMs with flexible activations

In this subsection we present some results for two deep Boltzmann machines (DBM) with three RBMs. The activation of the first visible layer is relu and the rest is identity, the activation of all hidden layers is softsign. The first DBM has the following configuration:

$$\text{RBM}(784, 784) \leftrightarrow \text{RBM}(784, 196) \leftrightarrow \text{RBM}(196, 49)$$

The results are

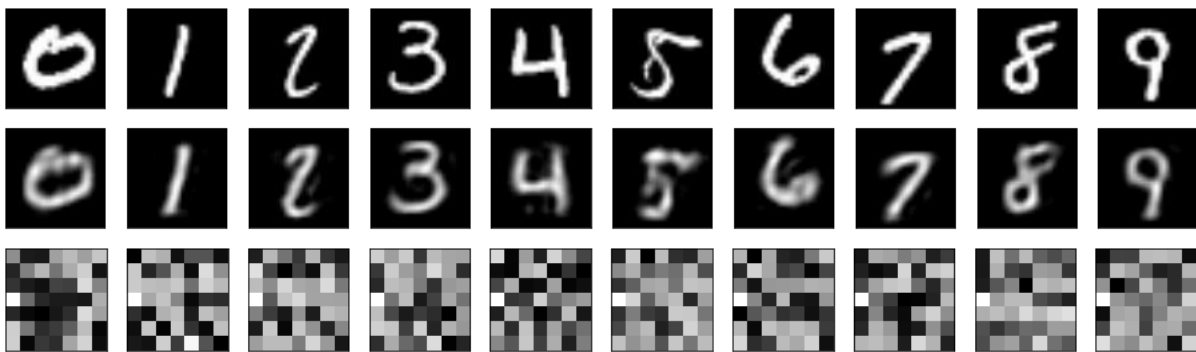


Fig 5. row 1: original images, row 2: reconstructed images and row 3: projected features

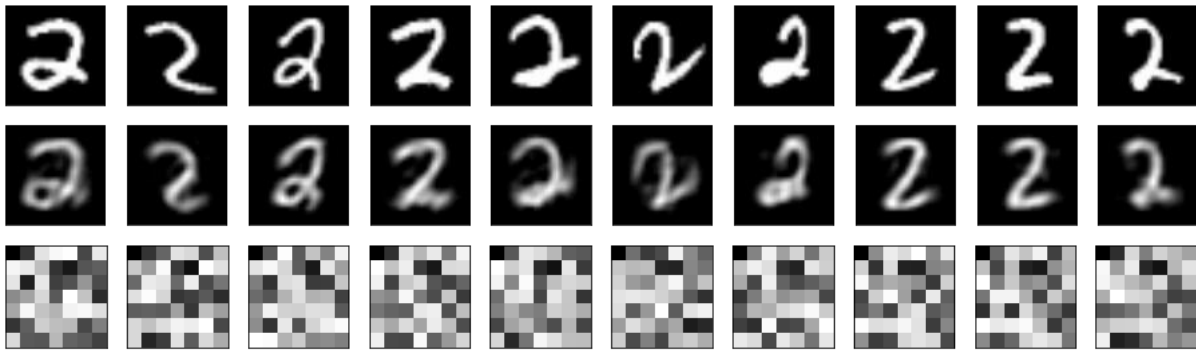


Fig 6. row 1: original images, row 2: reconstructed images and row 3: projected features

The second DBM has the following configuration:

$$\text{RBM (784, 784)} \leftrightarrow \text{RBM (784, 196)} \leftrightarrow \text{RBM (196, 16)}$$

The results are

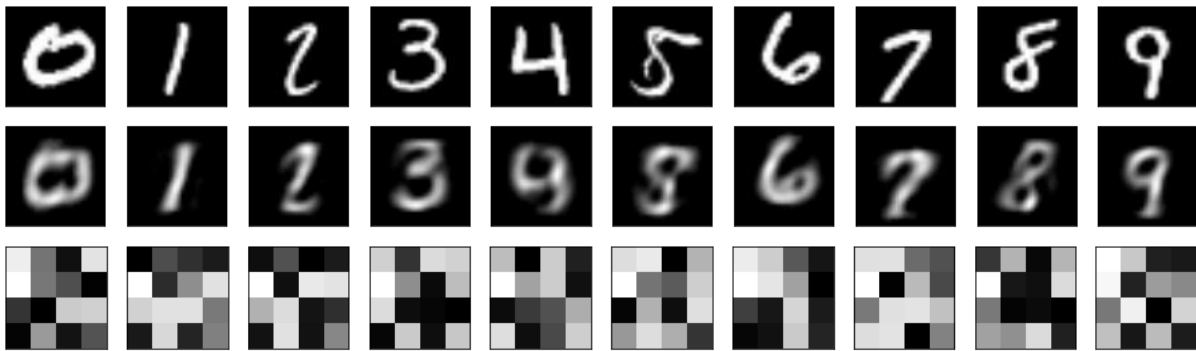


Fig 7. row 1: original images, row 2: reconstructed images and row 3: projected features

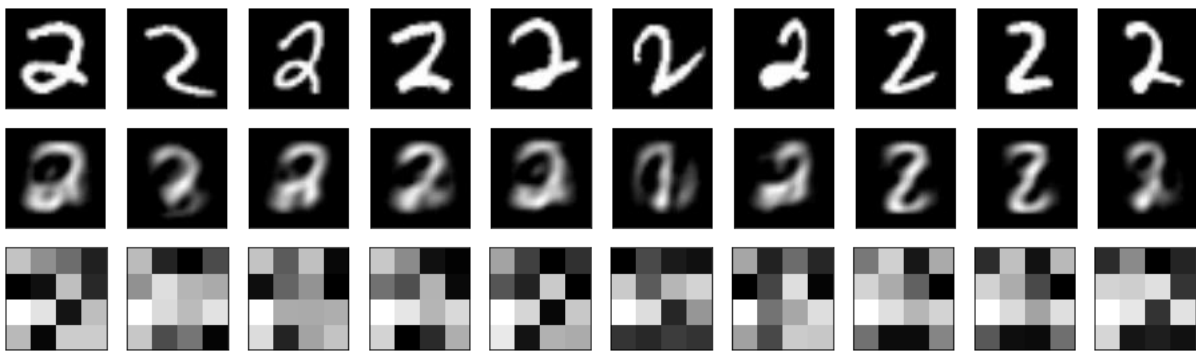


Fig 8. row 1: original images, row 2: reconstructed images and row 3: projected features

The numerical experiments in this subsection are focusing on the very low dimensions on the hidden layers which are different from [14] in which all layers have large number of dimensions. Notice that for the small dimension of 16 on the last layer, the reconstructed images look visually recognizable. More quantitative studies are under investigation on the optimization of parameters and architecture to improve the reconstruction accuracy.

V. Discussions

Though the probabilistic model has not been used in data mapping, here we try to give an interpretation of (3) by using the Gaussian distribution. We assume that the weights and biases on the hidden layer are all parameters, and the input data on the visible layer are observations of independent Gaussian random variables like the modeling for image processing in [9, 10]. We point out that the hidden layer is treated as parameters instead of random variables so that there is no need to define the probabilities. If the mean of the Gaussian variables on the visible layer can be estimated by

$$\bar{X} = \bar{A}_v(\mathbf{W}^T(\bar{A}_h(\mathbf{W}\bar{X} + \bar{B}_h)) + \bar{B}_v) \quad (19)$$

Then the likelihood of the observations to be the mean is

$$e^{-\frac{1}{2}|\bar{X} - \bar{X}|^2} = \exp\left(-\frac{1}{2}\left|\bar{X} - \bar{A}_v(\mathbf{W}^T(\bar{A}_h(\mathbf{W}\bar{X} + \bar{B}_h)) + \bar{B}_v)\right|^2\right) \quad (20)$$

Maximizing (20) is equivalent to (4).

Early applications of RBM were mostly focusing the image classification due to the value range requirements of Bernoulli distribution [15]. With the data mapping, the activation can be free to choose depending on the nature of the problem under consideration, so the data mapping may extend the applications of RBM to more diversified data [16-18]. A hybrid energy function is under investigation for the data mapping to perform the classification and regression.

Mathematically the projection from visible layer to hidden layer and the reconstruction from hidden layer to visible layer construct a pair of data mapping. The data mapping provides a unified framework on the linear and nonlinear data representation through choosing the node architecture and activation function. From the application perspective, the data mapping may give more options as to other existing methods from Bengio's review on the representation [19]. Through the minimization of squared errors (3) and (14), the mysterious CD1 is a finite difference approximation of the gradient descent after ignoring the second-order error. It was proved in [20] that the CD1 update direction is not the gradient of any function and was proved to be an approximation of gradient descent in this paper. The finite difference learning extends the application of CD1 to both undirected and directed graphs with flexible activations without needing a probabilistic interpretation. Within the data mapping framework, the RBM can handle the real-valued data in the same way on both visible and hidden layers, provides a new approach for data representation without using the covariance, and can admit non-sigmoid activations on both visible and hidden layers. Preliminary numerical experiments confirm the feasibility of data mapping on the dimensionality reduction, feature extraction and nonlinear representation. A package of python code and test data is available per request for readers to repeat the results (https://github.com/jshyou/Restricted-Boltzmann-Machine/blob/master/data_mapping/data_mapping.md). However more quantitative analysis is needed to optimize the network architecture and to fine tune the training parameters.

References

- [1] Goodfellow I., Bengio Y. & Courville A. C. (2015). *Deep learning*. MIT Press.
- [2] Smolensky P. (1986). Information processing in dynamical systems: foundations of harmony theory. In Rumelhart, D. E. & McLelland J. L. (Eds), *Parallel distributed processing: explorations in the microstructure of cognition, Volume 1: Foundations*, 194-281. MIT Press.
- [3] Hinton G. E. (2002). Training products of experts by minimizing contrastive divergence. *Neural Computation*, 14, 1771-1800.

- [4] Hinton G. E. & Salakhutdinov, R. R. (2006). Reducing the dimensionality of data with neural networks. *Science*, 313, 504–507.
- [5] Fischer A. & Igel C. (2014). Training restricted Boltzmann machines: An Introduction. *Pattern Recognition* 47, 25-39.
- [6] You J., Wang J. & Liang Z. (2007). Range condition and ML-EM checkerboard artifacts. *IEEE Trans. Nuclear Science*, 54, 1696-1702.
- [7] Hebron P. (2017). Restricted Boltzmann machine. <https://www.patrickhebron.com/learning-machines/week5.html>.
- [8] Gordon R., Bender R. & Herman G. T. (1970). Algebraic reconstruction techniques (ART) for three-dimensional electron microscopy and x-ray photography. *Journal of Theoretical Biology*, 29, 471–81.
- [9] Shepp L. A. & Vardi Y. (1982). Maximum likelihood reconstruction for emission tomography. *IEEE Trans. Medical Imaging*, 1, 113-122.
- [10] Hart H. & Liang Z. (1987). Bayesian image processing in two dimensions. *IEEE Trans. Medical Imaging*, 6, 201-208.
- [11] Hinton G. E. & McClelland J. L. (1987). Learning representations by recirculation. *NIPS*, 358-366.
- [12] Hérault J. & Ans B. (1984). Réseau de neurones à synapses modifiables : Décodage de messages sensoriels composites par apprentissage non supervisé et permanent. *Comptes Rendus de l'Académie des Sciences, Série III.*, 299, 525–528.
- [13] Coates A., Lee H. & Ng A. Y. (2011). An analysis of single-layer networks in unsupervised feature learning. *International Conference on Artificial Intelligence and Statistics (AISTATS)*, 15, 215-223.
- [14] Salakhutdinov R. R. & Hinton G. E. (2009). Deep Boltzmann machines. *Proceedings of the 12th International Conference on Artificial Intelligence and Statistics (AISTATS)*, 8, 448-455.
- [15] Larochelle H. & Bengio Y. (2008). Classification using discriminative restricted Boltzmann machines. *Proceedings of the 25th international conference on Machine learning*, 536-543.
- [16] Chopra P & Yadav S.K. (2015). Fault detection and classification by unsupervised feature extraction and dimensionality reduction. *Complex & Intelligent Systems*, 1, 25-33.
- [17] Kuremoto T., Kimura S., Kobayashi K. & Obayashi M. (2014). Time series forecasting using a deep belief network with restricted Boltzmann machines. *Neurocomputing*, 137, 47-56.
- [18] Nakashika T., Takaki S. & Yamagishi J. (2019). Complex-valued restricted Boltzmann machine for speaker-dependent speech parameterization from complex spectra. *IEEE Transactions on Audio, Speech, and Language Processing*, 27, 244-254.
- [19] Bengio Y., Courville A. & Vincent P. (2013). Representation learning: A review and new perspectives. *IEEE transactions on pattern analysis and machine intelligence* 35, 1798-1828.
- [20] Sutskever I. & Tieleman T. (2010). On the convergence properties of contrastive divergence. *Proceedings of the 13th International Conference on Artificial Intelligence and Statistics (AISTATS)*, 9, 789-795.